THE JOURNAL OF
PHYSICAL CHEMISTRY C

Article

pubs.acs.org/JPCC

Few-Layer Tin Sulfide: A New Black-Phosphorus-Analogue 2D Material with a Sizeable Band Gap, Odd−Even Quantum Confinement Effect, and High Carrier Mobility

Chao Xin,[†] Jiaxin Zheng,[†] Yantao Su, Shuankui Li, Bingkai Zhang, Yancong Feng, and Feng Pan*

School of Advanced Materials, Peking University Shenzhen Graduate School, Shenzhen 518055, China

Supporting Information

ABSTRACT: As a compound analogue of black phosphorus, a new 2D semiconductor of SnS layers is proposed. Based on state-of-the-art theoretical calculations, we confirm that such 2D SnS layers are thermally and dynamically stable and can be mechanically exoliated from α-phase SnS bulk materials. The 2D SnS layer has an indirect band gap that can be tuned from 1.96 eV for the monolayer to 1.44 eV for a six-layer structure. Interestingly, the decrease of the band gap with increasing number of layers is not monotonic but shows an odd−even quantum confinement effect, because the interplay of spin−orbit coupling and lack of inversion symmetry in odd-numbered layer structures results in anisotropic spin splitting of the energy bands. It was also found that such 2D SnS layers show high in-plane anisotropy and high carrier mobility (tens of thousands of $cm^2\ V^{-1}\ s^{-1}$) even superior to that of black phosphorus, which is dominated by electrons. With these intriguing electronic properties, such 2D SnS layers are expected to have great potential for application in future nanoelectronics.

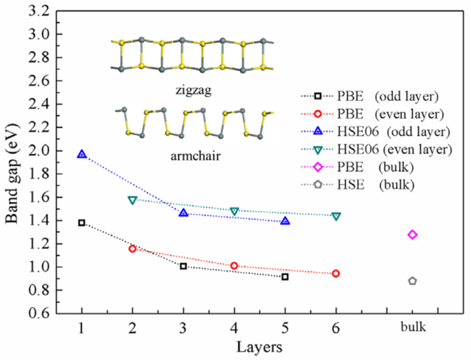

1. INTRODUCTION

Since the discovery of single-layer graphene, much effort has been devoted to the search for new two-dimensional (2D) nanoelectronic materials beyond graphene, such as by exfoliating stable, single-atom- or single-polyhedron-thick 2D materials from van der Waals solids.[1] One example is the recently extensively studied black phosphorus, which has attracted great interest because of its tunable band gap ($E_{g,bulk} \approx 0.3$ eV, $E_{g,monolayer} \approx 1$ eV) and high hole mobility ($\mu_{monolayer} \approx 1 \times 10^3\ cm^2\ V^{-1}\ s^{-1}$).[2,3] Even though this carrier mobility is lower than that of graphene (high carrier mobility of $\mu \approx 2 \times 10^5\ cm^2\ V^{-1}\ s^{-1}$ for a suspended sample),[4] achieving a tunable band gap is still a great challenge for graphene (zero band gap). Another well-studied family of van der Waals solids is the layered metal dichalcogenides (LMDCs), the most common being MoS_2.[5] The exfoliated 2D layers of LMDCs also display an array of unique properties, such as nanoelectronic and thermoelectric applications,[6] but unlike graphene, they have sizable band gaps that enable the fabrication of semiconductor devices including transistors, solar cells,[7] and thermoelectric materials.[8]

As a member of the LMDC family, the binary IV−VI compound SnS not only crystallizes in layered structures with van der Waals forces between layers consisting of strongly bonded Sn−S units but also is a compound analogue of black phosphorus and crystallizes in a similar layered structure (Figure 1a,b). Both of these materials have orthorhombic structures at low temperature but a more symmetric structure with space group *Cmcm* at high temperature.[9] All previous

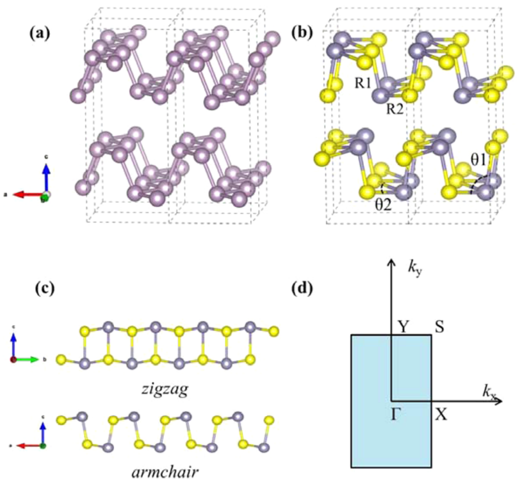

Figure 1. (a,b) Crystal structures of (a) bulk black phosphorus and (b) bulk black-phosphorus-analogue SnS marked with lattice vectors (*a*, *b*, *c*) and structural parameters (R_1, R_2, θ_1, and θ_2). (c) Crystal lattice of a monolayer of SnS viewed along two different directions: zigzag (parallel to *b*) and armchair (parallel to *a*). (d) Corresponding Brillouin zone.

Received: July 4, 2016
Revised: August 30, 2016
Published: September 7, 2016

DOI: 10.1021/acs.jpcc.6b06673
J. Phys. Chem. C 2016, 120, 22663−22669

studies on these materials mainly focused on the synthesis of nanostructures[10−13] and their applications in photovoltaics[14,15] because of their appropriate band gaps (1−1.6 eV), large absorption coefficients (>10^4 cm^{-1}), and low costs. Because SnS is an LMDC and a compound analogue of black phosphorus, investigations of its potential to be exfoliated as 2D layers and the corresponding physical properties would be very interesting. Tritsaris et al. studied the electronic structures of model single-layer, double-layer, and bulk structures of SnS using first-principles calculations.[16] They found that, compared with that of bulk SnS, the calculated band gaps were wider for fewer layers. However, they considered only single- and double-layer samples and did not show their stability as 2D materials. Brent et al. also calculated the optoelectronic characteristics of bulk and 10-layer to monolayer SnS using a quantum chemical density functional tight-binding approach and found that the band gap of SnS can be tuned by varying the number of SnS layers. However, they did not consider all odd-layer cases (considering only one-layer and three-layer structures) to provide a detailed overall relationship between band gap and number of SnS layers. Moreover, the above works also did not provide the carrier-transport properties in few-layer SnS.[17]

Actually, according to our calculations, the relaxed structure of odd-layer SnS belongs to the space group $Pmn2_1$ (No. 31, C_{2v}^7), whereas that of even-layer SnS retains *Pnma*. According to symmetry, bulk and even-layer SnS have an inversion center that is located at $(-x, -y, -z)$, whereas odd-layer SnS does not have. Monolayer SnS has a noncentrosymmetric polar site point group C_{2v}^7 for the Sn and S atoms. The C_{2v}^7 site point group and the noncentrosymmetry of odd-layer SnS would induce a spin polarization by spin−orbit coupling, corresponding to the Dresselhaus effect and a Rashba-like spin texture.[18] Thus, odd-layered and even-layered SnS would show different variation trends in electronic structures with number of layers.

In this work, we employ first-principles calculations to show that 2D SnS layers exfoliated from black phosphorus-like α-phase SnS can indeed exist. Considering spin−orbit coupling, we further calculate the electronic structures of few-layer (one to six layers) and bulk SnS. Interestingly, for the 2D SnS layers, the band gap does not fall monotonically with the thickness but shows an odd−even quantum confinement effect that results from different splittings of the energy bands and is associated with the symmetry variation. More importantly, such 2D SnS layers also show high in-plane anisotropy and high mobility (tens of thousands of cm^2 V^{-1} s^{-1}), even superior to that of black phosphorus. The sizable band gap and high carrier mobility make SnS layers very promising candidate nanoelectronic semiconductors for applications in future electronics.

2. CALCULATION DETAILS

We performed first-principles calculations and AIMD simulations based on density functional theory[19] as implemented in the Vienna ab initio simulation package (VASP).[20,21] We employed the Perdew−Burke−Ernzerhof functional revised for solids (PBEsol).[22] Considering the underestimation of band gaps in conventional DFT calculations, we repeated the PBE calculations using the Heyd−Scuseria−Ernzerhof (HSE06)[23] functional with 25% Fock exchange to predict a more accurate band gap, which is crucial for electronic properties. The calculations of spin−orbit splitting were performed using noncollinear calculations with fully relativistic pseudopotentials. The plane-wave energy cutoff was set to 450 eV. The valence configurations used for Sn and S were $4d^{10}5s^25p^2$ and $3s^23p^4$, respectively. Brillouin zone integrations were performed with the tetrahedron method in a 4 × 4 × 2 Monkhorst−Pack *k*-point mesh centered at Γ.[24] The ionic positions, lattice parameters, and unit-cell shape were sequentially relaxed to obtain the ground-state structure in such a way that the external pressure and the residual forces on each atom were less than 0.01 kbar and 0.001 eV/Å, respectively. For layer models, we used periodic boundary conditions along the *c* direction, with vacuum regions of 20 Å between adjacent images in the direction perpendicular to the layers. Convergence tests with greater vacuum spacing guaranteed that this size was sufficient to avoid spurious interactions between neighboring images. A DFT-D2 semiempirical dispersion-correction approach was employed to correct the van der Waals (vdw) interactions.[25] The convergence criterion of total energy was set to 1 meV in our AIMD simulations. Structure relaxations were performed without any symmetry constraints. Phonon properties were calculated using the finite displacement method implemented in Phonopy.[26] A 2 × 2 supercell was constructed to calculate the atomic forces using VASP, with a very high accuracy (stringent energy convergence croterion of 10^{-8} eV per unit cell).

3. RESULTS AND DISCUSSION

As one can see, bulk SnS is the compound analogue of elemental black phosphorus and crystallizes in a similar layered structure (Figure 1a,b). The symmetry group of their low-temperature crystal structures is *Pnma* (No. 62, D_{2h}^{16}) and resembles a distorted NaCl-type structure. Figure 1c shows monolayer SnS along the in-plane zigzag and armchair directions, as well as the corresponding 2D Brillouin zone with the high-symmetry *X* and *Y* points denoted in Figure 1d. It is necessary to optimize the structure of bulk SnS first because the structures of the SnS layers used in this work were cut from it. The optimized lattice parameters are $a = 4.505$ Å, $b = 3.993$ Å, and $c = 11.352$ Å, which are in good agreement with the experimental values ($a = 4.334$ Å, $b = 3.987$ Å, and $c = 11.199$ Å).[27] Owing to its layered structure, SnS also shows strong anisotropic vibrational properties, and samples exhibit significant differences in their physical characteristics when measurements are made along the three crystallographic directions. Table 1 shows the changes in geometrical structure as a function of the number of layers from 1 to 6. The length of the *b* axis increases by only 0.03 Å from six-layer to monolayer SnS, whereas *a* decreases by 0.06 Å. There is an abrupt reduction of *a* between few-layer and bulk SnS that can be attributed to the primary consequence of interlayer van der Waals interactions in few-layer and bulk SnS. The strength of bonding along the zigzag (*b*) direction is larger than that along the armchair (*a*) direction, so the *a* direction exhibits an abrupt reduction from

Table 1. Structural Parameters of Bulk and Few-Layer SnS

number of layers	a (Å)	b (Å)	Δc (Å)	R_1 (Å)	R_2 (Å)	θ_1 (deg)	θ_2 (deg)
bulk	4.52	4.01	2.72	2.66	2.68	104.17	96.33
1	4.31	4.04	–	2.59	2.71	102.68	95.07
2	4.34	4.02	2.81	2.63	2.69	103.04	95.85
3	4.34	4.02	2.80	2.66	2.68	103.29	95.85
4	4.36	4.02	2.80	2.66	2.68	103.40	95.88
5	4.38	4.00	2.80	2.66	2.68	103.40	95.82
6	4.39	4.01	2.78	2.66	2.68	103.44	95.75

bulk to few-layer SnS, whereas the b direction does not. The significant stretching of the a axis from one- to six-layer SnS systems was caused mainly by an increase in the bond angle θ_1.

The layers in SnS are coupled with weak van der Waals forces.[28] To visualize the hybridized electronic states between the Sn and S atoms, the electronic charge distributions of bulk, monolayer, and bilayer SnS were calculated (Figure 2). These bonding charge distributions clearly show the electron accumulation in SnS, and the amount of charge localized in this region qualitatively indicates the strength of the Sn−S bond. No bonding-like feature is visible in the interlayer region, indicating that van der Waals forces play the primary role in mediating the interlayer interaction, which explains the changes in the structural parameters from one layer to six layers.

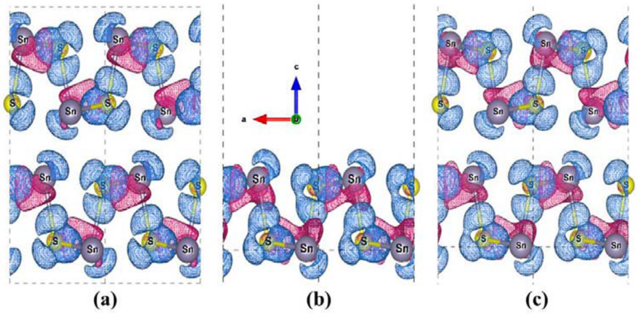

Figure 2. Charge density difference for SnS: (a) bulk, (b) monolayer, (c) bilayer. The blue isosurface represents electron accumulation, and the red isosurface represents electron depletion.

The interlayer binding energy (E_B) depends on the distance at which the interlayer is calculated, as illustrated schematically in Figure 3a,b. The E_B value of SnS calculated with PBE-D2 is 11.6 meV/Å, which is larger than that of graphene (10 meV/Å), but smaller than that of MoS_2 (15 meV/Å).[28] Therefore, 2D layered SnS can theoretically be obtained by mechanical exfoliation.[13] Recently, the liquid-phase exfoliation of tin(II) sulfide to produce bilayer SnS nanosheets in N-methyl-2-pyrrolidone was reported.[17]

To confirm the dynamical stability of bulk and few-layer SnS, the phonon dispersion was calculated in the framework of density functional perturbation theory.[29] The phonon bands of bulk, monolayer, and bilayer SnS are plotted in Figure 3c. No obvious imaginary mode can be seen in the first Brillouin zone, suggesting that bulk, monolayer, and bilayer SnS are dynamically stable.[30] The thermal stabilities of monolayer and bilayer SnS were further calculated using ab initio molecular dynamics (AIMD) simulations within the canonical ensemble. To explore possible structural rearrangement and decrease the constraint of periodic boundary conditions, the 2D structures were calculated with (4 × 4) and (6 × 6) supercells in the ab plane. After the samples had been heated at room temperature (300 K) for 1 ps with a time step of 1 fs, no structural disorder was found in all cases. Snapshots of atomic configurations of monolayer SnS at the end of AIMD calculations are plotted in the Figure 3d inset. Furthermore, calculations showed that the monolayer SnS structure can withstand temperatures as high as 1000 K and that bilayer SnS structure can also exist at 300 and 1000 K (Supporting Information, Figures SI1 and SI2), implying that it is hard for the 2D SnS to transform to other local phases. All of the above MD simulation data confirm that

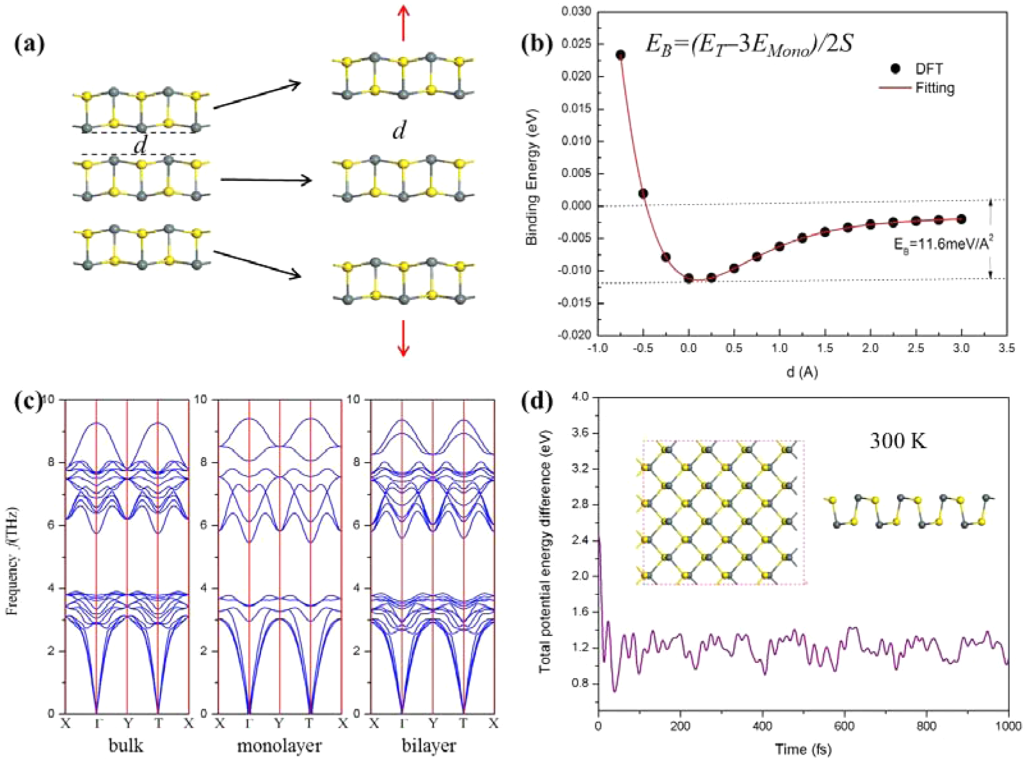

Figure 3. Dynamic and thermal stability. (a) Procedure for calculating the interlayer binding energy by increasing the interlayer distance, d. (b) Schematic illustration of a binding energy curve. (c) Phonon dispersion band structure along the high-symmetry k-point path in the first Brillouin zone. The high-symmetry k points are Γ (0, 0, 0), X (0.5, 0, 0), Y (0, 0.5, 0), and T (0.5, 0, 0.5). (d) Total potential energy fluctuations during AIMD simulations of monolayer SnS at 300 K. The insets show snapshots at 1 ps from the 4 × 4 supercell simulation.

DOI: 10.1021/acs.jpcc.6b06673
J. Phys. Chem. C 2016, 120, 22663−22669

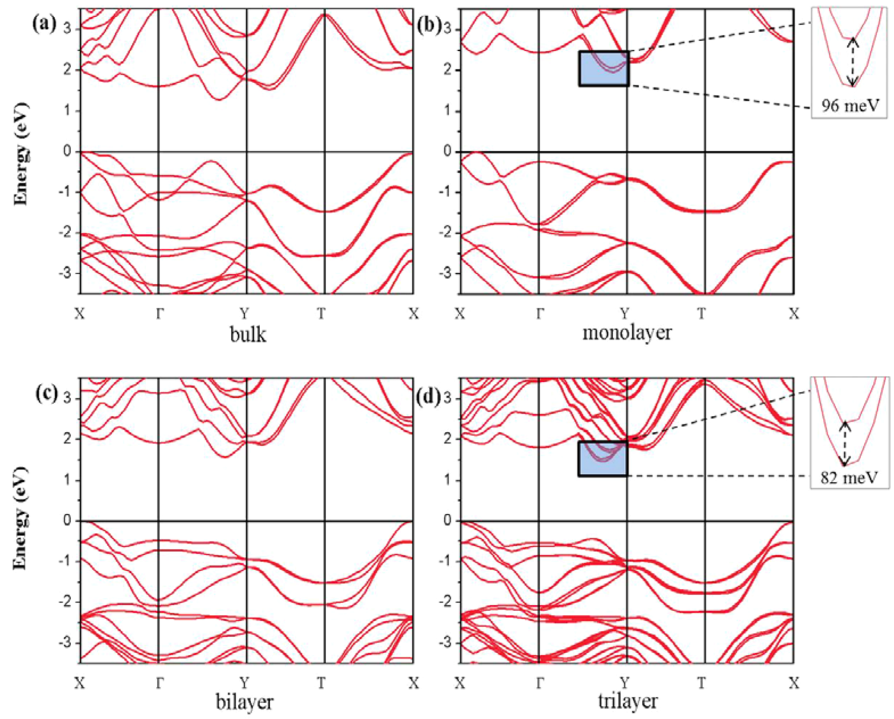

Figure 4. Electronic band structures of few-layer SnS: (a) bulk, (b) monolayer, (c) bilayer, and (d) trilayer SnS with the HSE06 correction and spin−orbit coupling effect. The insets show the spin−orbit split energies of monolayer and three-layer SnS.

the stability and Sn−S bonds in the structure of monolayer and bilayer SnS are very strong, despite the high temperature.

Tunable band gap energies within the visible range represent one of the most interesting properties of the group-IV monochalcogenides.[31,32] The calculated band structures of bulk, monolayer, bilayer, and trilayer SnS, including HSE06 and spin−orbit coupling corrections, are shown in Figure 4. The band gap of bulk SnS is indirect, with the valence-band maximum along Γ−*X* and the conduction-band minimum along Γ−*Y*. The value of the bulk SnS gap (1.27 eV) is in good agreement with optical absorption measurements (1.24 eV).[33] The calculated values for the energy gaps (E_g) of few-layer SnS (one to six layers) are summarized in Table 2 and Figure 5.

Table 2. Electronic Effective Mass (m_x^*, m_y^*) with Respect to the Free-Electron Mass

		electron		hole	
number of layers	HSE band gap (eV)	m_x^* (m_0)	m_y^* (m_0)	m_x^* (m_0)	m_y^* (m_0)
bulk	1.278	0.145	0.178	0.240	0.260
1	1.964	0.238	0.253	0.223	0.223
2	1.621	0.218	0.256	0.344	0.550
3	1.461	0.195	0.225	0.374	0.322
4	1.487	0.192	0.202	0.312	0.283
5	1.395	0.170	0.192	0.312	0.240
6	1.443	0.165	0.198	0.322	0.267

Their band structures were calculated along high-symmetry paths of the Brillouin zone (BZ) (Figure 1d). Compared with PBE band structures (Figure SI3), the HSE06 exchange-correlation functional opens the gap (Figure 4), whereas the band dispersion remains nearly unchanged. Monolayer SnS exhibits the largest band gap of 1.964 eV. The thinner the few-layer SnS system, the weaker the interlayer van der Waals interaction, and thus, the smaller the dispersion of bands, resulting in a larger band gap. Thus, the gap falls continuously upon the addition of more layers to the monolayer, reaching 1.443 eV in six-layer SnS, as shown in Figure 5.

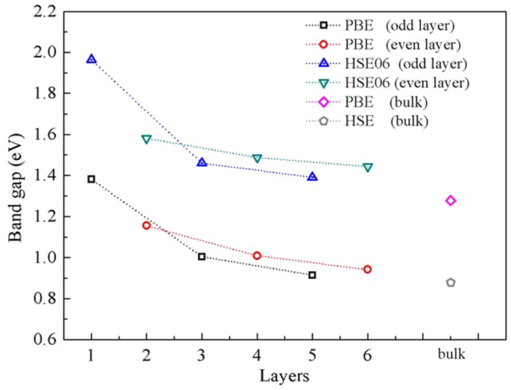

Figure 5. Evolution of the indirect band gaps as a function of the layer thickness. The PBE- and HSE06-calculated band gaps of the bulk are marked by a pink diamond and a gray pentagon, respectively.

However, in contrast to the normal quantum confinement effect in tunable-band-gap systems, the band gap does not fall monotonically with the thickness but shows an odd−even effect (Figure 5). Interestingly, it should be noted that there is a splitting of the energy bands at the conduction-band minimum (CBM) along Γ−*Y* for monolayer and trilayer SnS (Figure 4b,d), but not for bulk and bilayer SnS (Figure 4a,c), which would account for the odd−even effect in the band structures of few-layer SnS.

So why do the energy bands split at the CBM for odd-layered SnS? This can be explained in terms of the asymmetry of the crystal space group and a spin−orbit coupling effect. As mentioned in a previous section, whereas the bulk crystal and

DOI: 10.1021/acs.jpcc.6b06673
J. Phys. Chem. C 2016, 120, 22663−22669

Table 3. Predicted Carrier Mobility in 2D SnS

		deformation potential (eV)		2D elastic modulus (J m^{-2})		mobility[c] (10^3 cm^2 V^{-1} s^{-1})	
carrier type[a]	N_L[b]	E_{1x}	E_{1y}	C_{x_2D}	C_{y_2D}	μ_{x_2D}	μ_{y_2D}
e	1	1.50 ± 0.47	3.12 ± 0.47	110.39	64.70	10−38	1.7−3.2
	2	2.22 ± 0.46	2.38 ± 0.58	204.18	166.80	10−25	8.5−23
h	1	3.94 ± 0.59	5.58 ± 0.54	110.39	64.70	2.3−4.2	1.3−1.9
	2	7.28 ± 0.89	3.30 ± 0.57	204.18	166.80	0.1−0.5	0.1−0.9

[a] e, electron; h, hole. [b] N_L = number of layers. [c] Calculated using eq 1 with T = 300 K.

even-layered SnS have inversion points, the inversion symmetry is broken in the odd-layered structures. The C_{2v}^7 site point group and the noncentrosymmetry in odd-layered SnS would induce a spin polarization by spin−orbit coupling[26] and break the spin degeneracy of the band structures of odd-layered SnS leading to directionally dependent spin splitting at the CBM, as shown in Figure 4b,c. This splitting of the CBM along Γ−Y for monolayer SnS is 96 meV, which is larger than the splittings for SnSe and GeSe.[32] This band splitting due to spin−orbit coupling and the lack of inversion symmetry has also been reported for MoS_2 monolayers and other tranisition-metal dichalcogenides (TMDs) with small energy splitting values.[34] Thus, the spin−orbital splitting effect makes the band gap difference between odd- and even-layered SnS. Another explanation for the odd−even effect is as follows: The even numbered layers of SnS is antiferroelectric with a zero net polarization, whereas the polarization for odd-numbered layers is nonzero, where monolayer SnS was revealed to be ferroelectric with SOC band splitting, which will give rise to Rashba splitting.[37]

Further analysis shows that the CBM of monolayer SnS are mainly composed by Sn atom (Figure SI4), so the band of spin-splitting are originated from Sn. The valence band maximum (VBM) in bilayer is very flat, which is determined by the S atom.

The carrier effective mass of the band is a very important band parameter that is related with the dispersion of band and a critical part in dynamical properties of carriers. In the theory of transport in semiconductors, the carrier is treated as a classical particle with momentum and effective mass. The effective mass tensor is defined as[35]

$$[m^*]_{ij}^{-1} = a_{ij} = \pm\hbar^{-2}\left(\frac{\partial^2 E}{\partial k_i \partial k_j}\right) \tag{1}$$

In all of the few-layer SnS systems, the electron effective masses remain small (Table 2). For the Γ−X direction in the monolayer, the carrier effective masses are 0.238 m_0 (electron) and 0.253 m_0 (hole), only 0.04−0.05 m_0 larger than those in bulk SnS. It is remarkable that, in the Γ−X direction of bilayer SnS, the valence band appears to be nearly flat close to the X point, with an effective mass of 3.12 m_0 (see Figure 4c), 13 times its bulk value of 0.24 m_0. As a comparison, the effective mass for the conduction band of monolayer is 0.223 m_0, very close to its bulk value of 0.24 m_0. Unlike the the band gap, only the electron effective mass along Γ−Y exhibits a strongly layer-dependent variation: from 0.253 m_0 for the monolayer to 0.248 m_0 for the bilayer and finally to 0.198 m_0 in the six-layer system, close to the bulk value of 0.178 m_0. The small effective masses of few-layer SnS indicate the possible inheritance of high carrier mobility from the corresponding bulk materials.

The carrier mobility in 2D material can be estimated by the phonon-limited formula[3]

$$\mu_{2D} = \frac{e\hbar^3 C_{2D}}{k_b T m_e^* m_d (E_1^i)^2} \tag{2}$$

where m_e^* is the effective mass along the transport direction (either m_x or m_y along the x or y direction, respectively) and m_x is the average density-of-state mass defined as $m_d = \sqrt{m_x^* m_y^*}$. The deformation potential $E_1^i = \frac{\Delta V_i}{\Delta l / l_0}$ is computed from the energy change induced by the lattice compression or dilatation of few-layer SnS by a step of $\Delta l / l_0$ = 0.005 in the transport direction. What should be noted is that the E_1^i value of the valence band minimum (VBM, E_h) is for a hole and that of the conduction band maximum (CBM, E_e) is for an electron. Typical fitting results for E_{1x} (electron) and E_{1y} (hole state) are shown in Figures SI5 and SI6. The elastic modulus of the longitudinal acoustic mode C_{2D} in the propagation direction is defined as

$$\frac{E - E_0}{S_0} = C(\Delta l / l_0)^2 / 2 \tag{3}$$

where E and E_0 are the total energy with lattice changes in the i direction and at an equilibrium state, respectively, and the S_0 is the area of the 2D material at the equilibrium state.

According to eq 2, the extremely high carrier mobility includes three factors: large elastic moduli, small effective mass, and small deformation potentials. The calculated carrier mobilities of the monolayer and bilayer are listed in Table 3. The elastic moduli of monolayer SnS were nealy 110 and 65 J m^{-2} along the x and y directions, respectively, which are larger than those of monolayer black phosphorus[3] of 102 and 29 J m^{-2}. In detail, the deformation potential E_e (effective electron mass at the CBM) for SnS is 1.5 ± 0.47 eV (0.145 m_0), which is larger (smaller) than that for monolayer black phosphorus is 0.15 ± 0.03 eV (6.35 m_0) but is much smaller than that for 2D α-arsenic phosphide is 5.1 eV (1.1 m_0).[36] Our predicted electronic mobilities for the monolayer (x direction) and bilayer (y direction) SnS systems (Table 3) are very large (tens of thousands of cm^2 V^{-1} s^{-1}), asymmetric and anisotropic between electrons and holes, with the electron being more mobile in both directions. The electron mobility along x is 6−12 times larger than that along y, that is, 10000−38000 versus 1700−3200 cm^2 V^{-1} s^{-1}. These carrier mobilities are even superior to those of black phosphorus (10000−26000 and 640−700 cm^2 V^{-1} s^{-1}), making x the direction with higher electron conductivity. This large value for monolayer SnS is a consequence of the extremely small effective electron mass and large elastic moduli. Thus, the low deformation potential and effective mass and large elastic moduli are crucial to the high mobility of the black-phosphorus-analogue 2D material.

4. CONCLUSIONS

In summary, we have predicted a new 2D semiconductor of SnS layers, which can be exfoliated from the black-phosphorus-like α-phase SnS. Using hybrid functional calculations with spin−orbit coupling, we found that the band gap decreases from 1.96 eV for the monolayer to 1.44 eV for six layers and then to 1.24 eV for bulk SnS. However, this decrease of the band gap is not monotonic but shows an odd−even quantum confinement effect, because of a large splitting of the energy bands in the odd layers induced by the spin−orbit coupling and lack of inversion symmetry. The 2D SnS layers also show high mobilities (10000−38000 $cm^2 V^{-1} s^{-1}$ in the monolayer and 10000−25000 $cm^2 V^{-1} s^{-1}$ in the bilayer), which is even superior to black phosphorus (10000−26000 $cm^2 V^{-1} s^{-1}$ in the monolayer and 2600−2800 $cm^2 V^{-1} s^{-1}$ in the bilayer). However, unlike the more mobile holes in black phosphorus, the electrons are more mobile in such SnS layers. Moreover, similarly to black phosphorus, there is also high in-plane anisotropy for carrier mobilities. All of these results predict a new 2D semiconductor with an odd−even quantum confinement effect, high carrier mobility, and high in-plane anisotropy. We hope that these findings will motivate experimental efforts.

■ ASSOCIATED CONTENT

Ⓢ Supporting Information

The Supporting Information is available free of charge on the ACS Publications website at DOI: 10.1021/acs.jpcc.6b06673.

Total potential energy fluctuation during AIMD simulations of SnS, electronic band structures, and deformation potentials (PDF)

■ AUTHOR INFORMATION

Corresponding Author

*E-mail: panfeng@pkusz.edu.cn. Tel.: +86-755-26033200.

Author Contributions

†C.X. and J.Z. authors contributed equally.

Notes

The authors declare no competing financial interest.

■ ACKNOWLEDGMENTS

This work was financially supported by the National Project for EV Batteries (20121110, OptimumNano, Shenzhen, China), the National Natural Science Foundation of China (No. 11404011), a Guangdong Innovation Team Project (No. 2013N080), and Shenzhen Science and Technology Research Grants (Nos. ZDSY20130331145131323, JCYJ20140903101633318, JCYJ20140903101617271, JCYJ20150629144835001, and JCYJ20150331100515911).

■ REFERENCES

(1) Butler, S. Z.; Hollen, S. M.; Cao, L. Y.; Cui, Y.; Gupta, J. A.; Gutiérrez, H. R.; Heinz, T. F.; Hong, S. S.; Huang, J.; Ismach, A. F.; Johnston-Halperin, E.; Kuno, M.; Plashnitsa, V. V.; Robinson, R. D.; Ruoff, R. S.; Salahuddin, S.; Shan, J.; Shi, L.; Spencer, M. G.; Terrones, M.; Windl, W.; Goldberger, J. E. Progress, Challenges, and Opportunities in Two-Dimensional Materials beyond Graphene. *ACS Nano* **2013**, *7*, 2898−2926.

(2) Çakır, D.; Sevik, C.; Peeters, F. M. Significant Effect of Stacking on the Electronic and Optical Properties of Few-Layer Black Phosphorus. *Phys. Rev. B: Condens. Matter Mater. Phys.* **2015**, *92*, 165406.

(3) Qiao, J. S.; Kong, X. H.; Hu, Z. X.; Yang, F.; Ji, W. High-Monility Transport Anisotropy and Linear Dichroism in Few-Layer Black phosphorus. *Nat. Commun.* **2014**, *5*, 4475.

(4) Du, X.; Skachko, I.; Barker, A.; Andrei, E. Y. Approaching Ballistic Transport in Suspended Graphene. *Nat. Nanotechnol.* **2008**, *3*, 491−495.

(5) Peelaers, H.; Van de Walle, C. G. Effects of Strain on Band Structure and Effective Mass in MoS_2. *Phys. Rev. B: Condens. Matter Mater. Phys.* **2012**, *86*, 241401.

(6) Zhao, L. D.; Lo, S. H.; Zhang, Y. S.; Sun, H.; Tan, G. J.; Uher, C.; Wolverton, C.; Dravid, V. P.; Kanatzidis, M. G. Ultralow Thermal Conductivity and High Thermoelectric Figure of Merit in SnSe Crystals. *Nature* **2014**, *508*, 373.

(7) Vidal, J.; Lany, S.; d'Avezac, M.; Zunger, A.; Zakutayev, A.; Francis, J.; Tate, J. Band-Structure, Optical Properties, and Defect Physics of the Photovoltaic Semiconductor SnS. *Appl. Phys. Lett.* **2012**, *100*, 032104.

(8) Zhao, L.-D.; Tan, G.; Hao, S.; He, J.; Pei, Y.; Chi, H.; Wang, H.; Gong, S.; Xu, H.; Dravid, V. P.; Uher, C.; Snyder, G. J.; Wolverton, C.; Kanatzidis, M. G. Ultrahigh Power Factor and Thermoelectric Performance in Hole-Doped Single-Crystal SnSe. *Science* **2016**, *351*, 141−144.

(9) Ke, F.; Yang, J.; Liu, C.; Wang, Q.; Li, Y.; Zhang, J.; Wu, L.; Zhang, X.; Han, Y.; Wu, B.; Ma, Y.; Gao, C. High-Pressure Electrical-Transport Properties of SnS: Experimental and Theoretical Approaches. *J. Phys. Chem. C* **2013**, *117*, 6033−6038.

(10) Zhang, Y. J.; Lu, J.; Shen, S. L.; Xu, H. R.; Wang, W. B. Ultralarge Single Crystal SnS Rectangular Nanosheets. *Chem. Commun.* **2011**, *47*, 5226−5228.

(11) Vaughn, D. D.; Hentz, O. D.; Chen, S.; Wang, D.; Schaak, R. E. Formation of SnS Nanoflowers for Lithium Ion Batteries. *Chem. Commun.* **2012**, *48*, 5608−5610.

(12) Biacchi, A. J.; Vaughn, D. D.; Schaak, R. E. Synthesis and Crystallographic Analysis of Shape-Controlled SnS Nanocrystal Photocatalysts: Evidence for a Pseudotetragonal Structural Modification. *J. Am. Chem. Soc.* **2013**, *135*, 11634−11644.

(13) de Kergommeaux, A.; Lopez-Haro, M.; Pouget, S.; Zuo, J.-M.; Lebrun, C.; Chandezon, F.; Aldakov, D.; Reiss, P. Synthesis, Internal Structure, and Formation Mechanism of Monodisperse Tin Sulfide Nanoplatelets. *J. Am. Chem. Soc.* **2015**, *137*, 9943−9952.

(14) Nair, M. T. S.; Nair, P. K. Simplified Chemical Deposition Technique for Good Quality SnS Thin Films. *Semicond. Sci. Technol.* **1991**, *6*, 132.

(15) Avellaneda, D.; Nair, M. S. T.; Nair, P. K. Photovoltaic Structures Using Chemically Deposited Tin Sulfide Thin Films. *Thin Solid Films* **2009**, *517*, 2500.

(16) Tritsaris, G. A.; Malone, B. D.; Kaxiras, E. Optoelectronic Properties of Single-Layer, Double-Layer, and Bulk Tin Sulfide: A Theoretical Study. *J. Appl. Phys.* **2013**, *113*, 233507.

(17) Brent, J. R.; Lewis, D. J.; Lorenz, T.; Lewis, E. A.; Savjani, N.; Haigh, S. J.; Seifert, G.; Derby, B.; O'Brien, P. Tin(II) Sulfide (SnS) Nanosheets by Liquid-Phase Exfoliation of Herzenbergite: IV−VI Main Group Two-Dimensional Atomic Crystals. *J. Am. Chem. Soc.* **2015**, *137*, 12689.

(18) Zhang, X. W.; Liu, Q. H.; Luo, J. W.; Freeman, A. J.; Zunger, A. Hidden Spin Polarization in Inversion-Symmetric Bulk Crystals. *Nat. Phys.* **2014**, *10*, 387.

(19) Jones, R. O.; Gunnarsson, O. The Density Functional Formalism, Its Applications and Prospects. *Rev. Mod. Phys.* **1989**, *61*, 689.

(20) Kresse, G.; Furthmüller, J. Efficient Iterative Schemes for ab initio Total-Energy Calculations Using a Plane-Wave Basis Set. *Phys. Rev. B: Condens. Matter Mater. Phys.* **1996**, *54*, 11169.

(21) Kresse, G.; Joubert, D. From Ultrasoft Pseudopotentials to the Projector Augmented-Wave Method. *Phys. Rev. B: Condens. Matter Mater. Phys.* **1999**, *59*, 1758.

(22) Perdew, J. P.; Ruzsinszky, A.; Csonka, G. I.; Vydrov, O. A.; Scuseria, G. E.; Constantin, L. A.; Zhou, X.; Burke, K. Restoring the

Density-Gradient Expansion for Exchange in Solids and Surfaces. *Phys. Rev. Lett.* **2008**, *100*, 136406.

(23) Heyd, J.; Scuseria, G. E.; Ernzerhof, M. Erratum: "Hybrd Functionals Based on a Screened Coulomb Potential" [J. Chem. Phys. 118, 8207 (2003)]. *J. Chem. Phys.* **2006**, *124*, 219906.

(24) Monkhorst, H. J.; Pack, J. D. Special Points for Brillouin-Zone Integrations. *Phys. Rev. B* **1976**, *13*, 5188.

(25) Tkatchenko, A.; Scheffler, M. Accurate Molecular Van Der Waals Interactions from Ground-State Electron Density and Free-Atom Reference Data. *Phys. Rev. Lett.* **2009**, *102*, 073005.

(26) Togo, A.; Tanaka, I. First Pinciples Phonon Calculations in Materials Science. *Scr. Mater.* **2015**, *108*, 1−5.

(27) Ehm, L.; Knorr, K.; Dera, P.; Krimmel, A.; Bouvier, P.; Mezouar, M. Pressure-Induced Structural Phase Transition in the IV−VI Semiconductor SnS. *J. Phys.: Condens. Matter* **2004**, *16*, 3545−3554.

(28) Björkman, T.; Gulans, A.; Krasheninnikov, A. V.; Nieminen, R. M. van der Waals Bonding in Layered Compounds from Advanced Density-Functional first Principles Calculations. *Phys. Rev. Lett.* **2012**, *108*, 235502.

(29) Baroni, S.; de Gironcoli, S.; Dal Corso, A.; Giannozzi, P. Phonons and Related Crystal Properties from Density-Functional Perturbation Theory. *Rev. Mod. Phys.* **2001**, *73*, 515.

(30) Sahin, H.; Cahangirov, S.; Topsakal, M.; Bekaroglu, E.; Akturk, E.; Senger, R. T.; Ciraci, S. Monolayer Honeycomb Structures of Group-IV Elements and III-V Binary Compounds: First-Principles Calculations. *Phys. Rev. B: Condens. Matter Mater. Phys.* **2009**, *80*, 155453.

(31) Malone, B. D.; Kaxiras, E. Quasiparticle Band Structures and Interface Physics of SnS and GeS. *Phys. Rev. B: Condens. Matter Mater. Phys.* **2013**, *87*, 245312.

(32) Gomes, L. C.; Carvalho, A. Phosphorene Analogues: Isoelectronic Two Dimensional Group-IV Monochalcogenides with Orthorhombic Structure. *Phys. Rev. B: Condens. Matter Mater. Phys.* **2015**, *92*, 085406.

(33) Shi, G.; Kioupakis, E. Anisotropic Spin Transport and Strong Visible-Light Absorbance in Few-Layer SnSe and GeSe. *Nano Lett.* **2015**, *15*, 6926.

(34) Zhu, Z. Y.; Cheng, Y. C.; Schwingenschlogl, U. Giant Spin-Orbit-Induced Spin Splitting in Two-Dimensional Transition Metal Dichalcogenide Semiconductors. *Phys. Rev. B: Condens. Matter Mater. Phys.* **2011**, *84*, 153402.

(35) Ashcroft, N. W.; Mermin, N. D. *Solid State Physics*; Harcourt College Publishers: New York, 1976; p 228.

(36) Shojaei, F.; Kang, H. S. Electronic Structure and Carrier Mobility of Two-Dimensional α Arsenic Phosphide. *J. Phys. Chem. C* **2015**, *119*, 20210−20216.

(37) Wu, M. H.; Zeng, X. C. Intrinsic Ferroelasticity and/or Multiferroicity in Two-Dimensional Phosphorene and Phosphorene Analogues. *Nano Lett.* **2016**, *16*, 3236.

DOI: 10.1021/acs.jpcc.6b06673
J. Phys. Chem. C 2016, 120, 22663−22669